

Anomalous U(1) to Z_q cross-over in quantum and classical q -state clock models.

Pranay Patil,^{1,2,*} Hui Shao,^{3,†} and Anders W. Sandvik^{1,4,‡}

¹*Department of Physics, Boston University, 590 Commonwealth Avenue, Boston, Massachusetts 02215, USA*

²*Laboratoire de Physique Théorique, Université de Toulouse, CNRS, UPS, France*

³*Center for Advanced Quantum Studies, Department of Physics, Beijing Normal University, Beijing 100875, China*

⁴*Beijing National Laboratory for Condensed Matter Physics and Institute of Physics, Chinese Academy of Sciences, Beijing 100190, China*

We consider two-dimensional q -state quantum clock models with quantum fluctuations connecting states with all-to-all clock transitions with different matrix elements, including the case of transitions restricted to only the nearest clock states. We study the quantum phase transitions in these models using quantum Monte Carlo simulations and finite-size scaling, with the aim of characterizing the cross-over from emergent U(1) symmetry at the transition (for $q \geq 4$) to Z_q symmetry of the ordered state. As in classical three-dimensional clock models, the cross-over is governed by a dangerously irrelevant operator with scaling dimension $\Delta_q > 3$. We specifically study $q = 5$ and $q = 6$ models with different forms of the quantum fluctuations and different anisotropies in the classical models. In all cases studied, we find consistency with the expected classical XY critical exponents related to the conventional order parameter as well as the scaling dimensions Δ_q . However, the initial weak violation of the U(1) symmetry in the ordered phase, characterized by an angular Z_q symmetric order parameter ϕ_q , scales with the system size in an unexpected way. As a function of the system size (length) L in the close neighborhood of the critical temperature, $\phi_q \propto L^p$, where the known value of the exponent is $p = 2$ in the classical isotropic XY model. In contrast, for strongly anisotropic XY models and all the quantum models studied, we observe $p = 3$. For weakly anisotropic models we observe a cross-over from $p = 2$ to $p = 3$ scaling. The exponent p also directly impacts the exponent ν' characterizing the divergence of the U(1) length scale ξ' in the thermodynamic limit, according to the general relationship $\nu' = \nu(1 + |y_q|/p)$, where ν is the exponent governing the conventional correlation length ξ and $y_q = 3 - \Delta_q$ is the scaling dimension of the clock field. We present a phenomenological argument for the $p = 3$ scaling behavior based on the renormalization of the clock field in the presence of anisotropy.

I. INTRODUCTION

Emergent symmetry at quantum phase transitions in condensed matter systems has been the subject of numerous discussions in recent literature [1–20]. Such symmetries are not apparent at the microscopic level and are typically associated with a second macroscopic length scale ξ' as a consequence of a so-called dangerously irrelevant (DI) perturbation [21–23]. This symmetry cross-over length diverges faster upon approaching a critical point than the conventional correlation length ξ . The scenario of deconfined quantum-critical points in two-dimensional (2D) quantum magnets is a prominent example [5–17], where a DI operator leads to emergent U(1) symmetry [6] of the Z_4 [7, 8, 24] or Z_3 [9, 25] (depending on the lattice) order parameter of a dimerized (valence-bond solid, VBS) phase.

DI perturbations of this kind are better known from classical models, with a prototypic example being three-dimensional (3D) q -state clock models with $q \geq 4$ [26–36, 38]. The discreteness of the allowed spin angles, or the presence of a soft q -fold symmetric potential, constitutes an irrelevant perturbation of the XY spin model

at the critical point, where the angular fluctuations of the course-grained order parameter become more uniform with increasing length scale. The “dangerous” aspect of the problem pertains to the ordered phase, where the clock perturbation becomes relevant and the symmetry crosses over from U(1) to Z_q (illustrated in Fig. 1) at the second length scale ξ' (and on a more technical level to

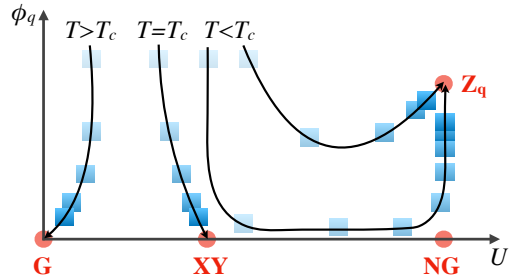


FIG. 1. Schematic Monte Carlo flow diagram for the 3D clock model [38] in the space of the Binder cumulant U and the Z_q order parameter ϕ_q . Darker squares denote larger system sizes and the flow is from small to large sizes. The fixed points are the paramagnetic Gaussian point G (reached for $T > T_c$), the critical point XY (reached at T_c), the ordered U(1) symmetric NG point (which the system approaches closely if $T < T_c$ in the neighborhood of T_c), and the ordered Z_q symmetric point (reached asymptotically for all $T < T_c$).

* pranayp@bu.edu

† huishao@bnu.edu.cn

‡ sandvik@bu.edu

a non-analytic scaling function of the dangerously irrelevant field in the original context were the concept was developed [21–23]).

In this paper we introduce a family of 2D quantum clock models and study the expected emergent U(1) symmetry previously studied in classical clock models. We analyze renormalization group (RG) flows versus the system size of observables computed using quantum Monte Carlo simulations, following methods recently developed in a study of classical 3D clock models [38]. A schematic flow diagram is shown in Fig. 1. While we find critical behavior with exponent compatible with the 3D XY universality class, as expected [39, 40], we also observe an intriguing violation of the expected relationship between the two length scales ξ and ξ' . To elucidate this surprising aspect of the quantum systems, we also study spatially anisotropic 3D classical XY models, where a stronger coupling in one dimension mimics the imaginary time dimension of the quantum models [39]. Here we observe cross-overs between the behavior of the isotropic model and that of the quantum models, suggesting that anisotropy affects the RG flow of the dangerously irrelevant perturbation in the ordered phase.

In the remainder of this introductory section we provide some additional background and motivations for our study. In Sec. IA we discuss recent interests in emergent symmetries in quantum systems in the context of deconfined quantum critical points. In Sec. IB we describe known facts on scaling behaviors related to emergent U(1) symmetry. In Sec. IC we outline the organization of the rest of the paper.

A. Emergent symmetries and deconfined criticality

The emergence and breaking of U(1) symmetry has been observed in $S = 1/2$ J - Q quantum spin models on the two-dimensional (2D) square and honeycomb lattices. These models harbor a deconfined quantum critical point separating Néel antiferromagnetic and VBS states breaking either Z_4 (square lattice) [7, 8, 12, 24] or Z_3 (honeycomb lattice) [9, 25] symmetry. The Néel and VBS phases correspond to condensed and confined phases, respectively, of the deconfined spinons that exist as independent objects only at the critical point [5], and the spinon confinement scale is also related to the second length-scale ξ' [12, 41]. The most concrete manifestation of the second length scale may be in the width of a domain wall separating domains with different VBS (or classical clock) patterns [6, 41]. The related energy density of the finite-size scaling of the critical domain walls exhibits puzzling differences between classical clock models and the J - Q model, which can be described phenomenologically with a scaling function with two relevant arguments if a certain limiting behavior is imposed when the system size is taken to infinity [12].

The emergent U(1) symmetry has also been investigated with a 3D classical loop model [11] and dimer mod-

els [17], which are also argued to realize deconfined quantum criticality. Signs of even higher symmetries, SO(5) and O(4), of the combined Néel and VBS order parameters have been observed in both the 2D quantum and 3D classical effective models [10, 13–15, 17], including in the surprising context of first-order Néel–VBS transitions resembling spin-flop transitions in O(N) models [18–20]. The break-down of the higher symmetries inside the ordered phases adjacent to the deconfined critical point should also be governed by a second length scale, which, however, has not been investigated extensively except in the case of the emergent O(4) symmetry at a first-order transition [18]

B. Scaling of emergent U(1) symmetry

The detailed form of the divergence of the second length scale ξ' is associated with subtleties even in the prototypical classical 3D clock models. The conventional correlation length ξ and the U(1) length (which also grows with the number of clock directions q) diverge as

$$\xi \sim |t|^{-\nu}, \quad (1a)$$

$$\xi'_q \sim t^{-\nu'_q} \quad (t > 0), \quad (1b)$$

where $t = (T_c - T)/T$ is the reduced distance to the critical temperature T_c and Eq. (1b) applies only to the ordered phase, $t > 0$, as indicated. The relationship between ν and ν'_q follows from a two-stage renormalization procedure [22, 23], where initially the system for small $t > 0$ flows toward the U(1) symmetry-breaking Nambu-Goldstone (NG) fixed point before the clock perturbation becomes relevant and the system crosses over and begins flowing toward the ordered clock fixed point with Z_q symmetry breaking.

In an early work, Chubukov *et al.* already derived what turns out to be the correct exponent relationship,

$$\nu' = \nu \left(1 + \frac{|y_q|}{p} \right), \quad (2)$$

where $y_q < 0$ is the scaling dimension of the irrelevant clock field at the critical point and $p = 2$ was determined from the properties of the NG point. However, this result appears to have been initially largely neglected, and other relationships were also subsequently proposed [28, 29]. More recent works have also arrived at Eq. (2) with $p = 2$ [32, 35], but the same form with $p = 3$ was argued in Ref. [31]. Very recently it was shown that Eq. (2) also follows from a generic scaling hypothesis with two relevant scaling arguments, $tL^{1/\nu}$ and $tL^{1/\nu'}$, but the exponent p depends on the physics of the system in a non-generic way [38]. A simple way to understand the exponent p in finite-size systems is that it governs the initial growth of a properly defined Z_q order parameter ϕ_q [which vanishes if the angular fluctuations of the order parameter are U(1) symmetric] when the clock perturbation becomes relevant; $\phi_q \sim L^p$ [31, 38].

C. Aims and paper outline

As already mentioned above, emergent U(1) and even higher symmetries are of great current interest in the context of VBS order in quantum magnets with putative deconfined quantum critical points. The U(1) symmetry emerging on the VBS side of the transition has been observed and the exponent ν' has been extracted using different methods in J - Q models with SU(2) spins as well as with generalizations to SU(N) symmetry [12, 31]. However, the recently proposed phenomenological scaling function [38] from which the relationship Eq. (2) can be derived offers improved ways of extracting the exponents, including p , from numerical data. This motivates more detailed studies of various models.

Our goal here is to consider perhaps the simplest quantum models with emergent U(1) symmetry—a family of 2D $S = 1/2$ quantum clock models. We find that Eq. (2) holds at the quantum phase transition, but with the exponent $p = 3$ instead of $p = 2$. Since the 2D quantum clock model should correspond to a spatially anisotropic classical 3D clock model, where the third dimension corresponds to imaginary time in the quantum case [39], we also study the classical clock model with varying degree of anisotropy. Here we find a cross-over behavior, where systems with weak anisotropy initially exhibit $\phi_q \sim L^2$ scaling in the neighborhood of T_c but for larger sizes cross over to $\phi_q \sim L^3$. The cross-over L decreases when the anisotropy increases, so that for a strongly anisotropic system no clear-cut L^2 scaling can be observed. Conversely, when the degree of anisotropy decreases, the cross-over length increases, so that the isotropic system only exhibits L^2 behavior. The cross-over behavior is also reflected in the t dependence of the cross-over length, and all our results point consistently to Eq. (2) with $p = 3$ as the correct way to describe the asymptotic relationship between ξ and ξ'_q . We do not have a detailed understanding of this surprising results but will present a phenomenological explanation hinting at the way anisotropy affects the renormalization of the clock field.

The structure of the paper is as follows: In Sec. II we review emergent symmetry in the context of the classical clock model, define the U(1) order parameter, and describe the finite size scaling method used to extract the scaling dimension associated with it. This is followed by a motivation for the anisotropic version of the same through the Suzuki-Trotter formalism in Sec. III, along with our numerical evidence for qualitatively different behaviors for varying degrees of anisotropy. We also present a phenomenological argument justifying the observed behaviors. These results are reinforced in Sec. IV, where analyses are presented for the emergence and breaking of U(1) symmetry at the ground state phase transitions of quantum clock models. In Sec. V we present results for the finite-size scaling of the critical domain wall energy of the quantum clock models. Conclusions and potential future directions of research are presented in Sec. VI. Auxiliary results are presented in two Appendices.

II. DANGEROUSLY IRRELEVANT OPERATOR IN THE CLASSICAL CLOCK MODEL

The classical 3D clock model is a prime example of emergent U(1) symmetry. It has been studied analytically [27, 29, 35] and in several numerical works [28, 30–34, 36, 38]. The Hamiltonian is the same as the standard XY model, namely

$$H_J = -J \sum_{\langle i,j \rangle} \cos(\theta_i - \theta_j), \quad (3)$$

with the additional constraint that θ_i is no longer a continuous angle but can only take one out of q equally spaced values, $\{0, 2\pi/q, 4\pi/q, \dots\}$. We call this the hard clock model, as the degree of freedom on a lattice site is discretized. Another way of formulating the clock model is by allowing the phase at each site to continuously vary between 0 and 2π as in the XY model, but including a site potential of the form

$$H_h = -h \sum_i \cos(q\theta_i) \quad (4)$$

to the XY Hamiltonian. We call the Hamiltonian $H = H_J + H_h$ the soft clock model, and clearly the hard model is obtained from it for $h \rightarrow \infty$. Both the hard and soft models exhibit 3D XY universality with emergent U(1) symmetry for $q \geq 5$ [26]. For $q = 4$, the hard model maps onto two decoupled Ising models and is different from the soft model, the latter exhibiting emergent U(1) symmetry for small values of h (with the exact bound on h not known precisely [25, 38]), while the former undergoes a conventional Ising transition with no emergent higher symmetry. From this point onwards, we only consider the hard clock model and simply refer to it as the clock model.

A. Renormalization of the clock field

As the low temperature phase must necessarily break the discrete Z_q symmetry, the corresponding operator perturbing the U(1) symmetric model behaves as a dangerously irrelevant operator [22, 23] as already discussed above in Sec. I B. The scaling dimension of the irrelevant clock operator is Δ_q and the corresponding negative scaling dimension of the field h is $y_q = 3 - \Delta_q$ according to standard scaling theory. Thus, at the critical point the effective field when course-grained at some length scale Λ is $h\Lambda^{y_q}$. While irrelevant at the critical point, away from the critical point the perturbation becomes relevant, which can be understood [23] as a scaling correction to the irrelevant part of the form $ht\Lambda^{1/\nu'_q}$, which eventually becomes the dominant contribution when $ht \neq 0$. This scaling variable defines the positive exponent ν'_q in the same way as the regular relevant (thermal) field t scaling as $t\Lambda^{1/\nu}$: When set to constants, the scaled fields give $\Lambda \propto \xi \sim t^{-\nu}$ and $\Lambda \propto \xi'_q \sim (ht)^{-\nu'_q}$, respectively, defining

the correlation length ξ and the length scale ξ'_q on which the clock perturbation becomes relevant. Since normally the microscopic field h is a constant, we can also simply write $\xi'_q \sim t^{-\nu'_q}$, though it should be kept in mind that there is also an h dependence in the overall effects of the clock perturbation.

Thus, there are two divergent length scales as the critical points is approached in the ordered phase: ξ associated with the fluctuations of the magnetization amplitude and ξ'_q associated with the cross-over from U(1) symmetric order on small length scales and Z_q symmetry on length scales ξ'_q and above. An important aspect of the problem is that the exponents ν and ν'_q are related according to Eq. (2) with $p = 2$, where the latter exponent is associated with the physics of the NG point. In this paper we will present evidence of p changing to $p = 3$ in the spatially anisotropic 3D XY model studied in Sec. III as well as in the quantum clock models introduced and studied in Sec. IV. We here first discuss the isotropic classical case in more details, reviewing the Monte Carlo RG flow method of Ref. [38] and also presenting some additional results not discussed there.

B. Order parameters

Using the magnetization

$$\vec{m} = \frac{1}{N} \sum_{i=1}^N \vec{m}_i, \quad m = |\vec{m}| \quad (5)$$

the standard Binder cumulant is defined as

$$U_m = \left(2 - \frac{\langle m^4 \rangle}{\langle m^2 \rangle^2} \right). \quad (6)$$

The development of magnetic order can be conveniently probed using U_m , as it vanishes for $L \rightarrow \infty$ in the paramagnetic phase and approaches unity when the magnetization develops a finite value with small fluctuations around this value in the ordered phase. At the critical point, U_m attains a non-trivial value between zero and unity, which is dependent on the universality class of the transition. These three fixed points allow us to probe the behavior of the relevant (thermal) field close to criticality.

We quantitatively analyze the emergent symmetry using an U(1) order parameter defined as

$$\phi_q = \langle \cos(q\theta) \rangle, \quad (7)$$

where θ is the orientation of the global magnetization vector \vec{m} . In the ferromagnetic phase, θ can only take the values of $\frac{2\pi i}{q}$ with i being an integer in the set $\{0, \dots, q-1\}$ and ϕ_q under this distribution of θ evaluates to unity. In the opposite extreme limit, if \vec{m} is circularly symmetric, θ is sampled from a uniform distribution and ϕ_q vanishes. Note that this quantity is not explicitly sensitive to the magnitude of the magnetization, only its orientation, though implicitly ϕ_q is still suppressed when m

is small in finite systems, as both the angular and amplitude fluctuations increase when the critical point is approached from below.

We note here that the Z_q order has in some past works also been investigated with an order parameter $\langle m \cos(q\theta) \rangle$ that also incorporates the magnitude of the conventional order parameter [31, 34]. This quantity was analyzed under the assumption (which also was demonstrated analytically in a certain limit) that the magnitude factors out; $\langle m \cos(q\theta) \rangle \rightarrow \langle m \rangle \langle \cos(q\theta) \rangle$, with $\langle m \rangle$ obeying the standard finite-size scaling form, $\langle m \rangle \sim L^{-\beta\nu}$ (β being the critical exponent of the magnetization below T_c) when m is small. While in Ref. [31], this procedure for $q = 4, 5, 6$ models delivered results for ν'_q consistent with later studies using Eq. (7) [32, 38], in Ref. [34] a very different result was obtained for $q = 6$. The reasons for the latter discrepancy is still unclear, but in general we advocate Eq. (7) as a pure Z_q order parameter that is not contaminated by potential effects of incomplete decoupling with the magnitude of the magnetization, and not requiring m to be small and obeying critical scaling governed by β/ν . Indeed this scaling breaks down if $\xi < L < \xi'_q$, whence m in a finite system can attain a finite value even when ϕ_q is still U(1) symmetric. In this regime (and also for $L > \xi'_q$) the assumptions used in Refs. [31, 34] are strongly violated [42].

C. RG flows and scaling function

Using ϕ_q and U_m , we can investigate four different regions which we find in our phase diagram using a flow diagram of the form shown schematically in Fig. 1, where each trajectory is for a particular value of $t = T - T_c$ and corresponds to a set of system sizes. A small size marks the start of the trajectory and increasing system size corresponds to lowering the energy scale (and of course increasing the course-graining length scale). Pictorially, such a diagram looks very much like a standard RG flow diagram (see, e.g., Ref. [32]), but it should be stressed that we are not looking at the flow of couplings, but of operators conjugate to those couplings that are directly accessible in simulations. Two of the regions indicated in Fig. 1 correspond to the paramagnetic phase ($U_m = 0$, $\phi_q = 0$) and the ferromagnetic phase ($U_m = 1$, $\phi_q = 1$) and are stable fixed points when viewed from a RG perspective. The other two regions are found in a vanishingly small vicinity of the critical point and correspond to the unstable critical point $U_m = c$, $\phi_q = 0$, where the magnetization develops power law correlations (and where the constant c itself is a universal number), and the unstable U(1) symmetric point $U_m = 1$, $\phi_q = 0$. This unstable point is the NG point and serves as the fixed point for the ordered 3D XY phase, which is never reached in the clock model but attracts the flow to its close neighborhood if T is close to T_c . The U(1) symmetric point has a finite magnetization magnitude as $U_m = 1$ and $\phi_q = 0$ asymptotically.

An actual flow diagram based on high-quality simulation data for the $q = 6$ clock model was presented in Ref. [38], and various aspects of the flow were tested to confirm the validity of an asymptotic scaling form

$$\phi_q \sim \Phi(tL^{1/\nu}, htL^{1/\nu'_q}, hL^{-|y_q|}), \quad (8)$$

describing the finite-size flows with two relevant arguments and one scaling correction due to the irrelevant clock field. Since $\phi_q = 0$ if $h = 0$, an expansion in the irrelevant argument gives

$$\phi_q \sim hL^{-|y_q|}\Phi(tL^{1/\nu}, htL^{1/\nu'_q}, 0), \quad (9)$$

which for fixed h (which has an undetermined value in the hard clock models used here) we simply use in the form of

$$\phi_q \sim L^{-|y_q|}\Phi(tL^{1/\nu}, tL^{1/\nu'_q}), \quad (10)$$

without the proportionality constant h (and note that there are also other, unknown proportionality constants).

Following the schematic flow diagram in Fig. 1 and the quantitative scaling function Eq. (9) it can be seen that two approximately scale invariant regions of the flow diagram can be identified. The standard critical scale-invariant behavior $\phi_q \sim L^{-|y_q|}$ applies when $tL^{1/\nu} \ll 1$, i.e., for $L \ll \xi$ (exemplified in Fig. 1 by the $T = T_c$ curve). For $tL^{1/\nu}$ not small but $tL^{1/\nu'_q} \ll 1$, which corresponds to $\xi \ll L \ll \xi'_q$, the second relevant argument in (10) can still be neglected, while the first one must result in a power-law behavior; thus $\phi_q \sim L^{-|y_q|}(tL^{1/\nu})^a$ for some exponent a on which we will elaborate further below. Here ϕ_q is small (which in Fig. 1 is just indicated by the segment very close to the horizontal axis of one of the $T < T_c$ curves), and the Binder cumulant flows towards 1 as the relative fluctuations of m diminish with increasing system size. Choosing a small value of t is necessary in order to attain the large separation in the length scales ξ and ξ_q that is required to clearly observe this second scaling region, and this becomes easier for larger q as ν'_q/ν increases with increasing q .

The second scale invariant flow can take us arbitrarily close to the NG point by choosing t sufficiently small and using sufficiently large system sizes. When tL^{1/ν'_q} is no longer small, i.e., L is of order ξ'_q or larger, we can write the scaling form Eq. (10)

$$\phi_q \approx L^{-|y_q|}(tL^{1/\nu})^a g(tL^{1/\nu'_q}), \quad (11)$$

which captures the flow away from the NG fixed point. It is useful to recast this expression more explicitly in terms of an exponent p governing the size dependence, $\phi_q \propto L^p$, when tL^{1/ν'_q} is still small and the flow approaches the NG fixed point. Then

$$\phi_q \approx L^p t^{\nu(p+|y_q|)} g(tL^{1/\nu'_q}), \quad (12)$$

and we will no longer refer to the exponent $a = \nu(p+|y_q|)$ in Eq. (11).

Further constraints on this form can be set by considering the final RG state $\phi_q \rightarrow 1$, where the L and t dependence should vanish. This necessitates $g \rightarrow (tL^{1/\nu'_q})^b$, with the exponent b chosen so that the powers of t and L in Eq. (12) are canceled, which is possible only also ν'_q is constrained by the values of p and $|y_q|$. These arguments result in the relationship between ν and ν'_q in Eq (2), but to further determine the value of p requires analysis of the physics of the NG point.

D. Cross-over from the NG point

The relationship Eq (2) had already been demonstrated with $p = 2$ by Chubukov *et al.* [27] (in their Appendix B) by using the scaling form for the transverse susceptibility of the system, which should deviate from the NG form when the observed length scale (the inverse of momentum chosen in the susceptibility) exceeds ξ'_q . Later works have also justified $p = 2$ [32, 35] in related ways. A contradictory result with $p = 3$ has also been argued [31] for, by suggesting that the dominant patterns have blocks which are XY ordered with a correlation length set by the XY fixed point. The analysis of the Monte Carlo RG flows in Ref. [38] agreed with $p = 2$ to a precision of a few percent.

We will build on the approach by Chubukov *et al.* [27] when we consider anisotropic systems in Sec. III. For completeness, we review their argument for $p = 2$ here and with some more details on the form of the transverse susceptibility in Appendix A. The starting point of the argument is that the Goldstone modes are well defined at the point where the RG flow approaches close to the NG fixed point [27]. The response to the discrete symmetry breaking $h \cos(q\theta)$ can be understood through the transverse susceptibility. Following the arguments presented in Appendix B of Ref. [27] and discussed in more detail in our Appendix A, the transverse susceptibility of a system with a macroscopic magnetization pointing along $\theta = 0$ is qualitatively controlled by the universal function

$$f(\bar{k}, \bar{h}) \propto \frac{1}{\bar{k}^2 + \bar{h}}. \quad (13)$$

Here \bar{k} and \bar{h} are dimensionless quantities related to the physical momentum and field through $\bar{k} \approx k\xi$, and $\bar{h} \approx h\xi^{y_q}$, respectively. Qualitative control of this function shifts from \bar{k} to \bar{h} at $\bar{k} \approx \bar{h}^{1/2}$. Using the relationship between \bar{k} and \bar{h} derived above, we obtain $k\xi \approx \xi^{y_q/2}$. To rewrite this relation in terms of ν and ν'_q , we first set k to be the inverse length scale $1/\xi'_q$ associated with the U(1) symmetry breaking, and next replace $\xi(\xi'_q)$ with $t^{-\nu}(t^{-\nu'_q})$. This leads to the relation between the two correlation length exponents in Eq. (2) with $p = 2$, for small ϕ_q close to the NG fixed point.

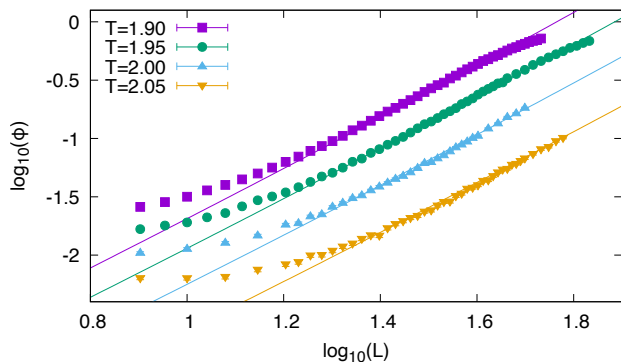


FIG. 2. Scaling of isotropic 3D XY Monte Carlo results for ϕ_6 with the linear system size L . The lines in this log-log plot are of the form $\phi_6 = aL^2 t^{\nu(p+|y_q|)}$ with $y_6 = -2.509$ [36], $p = 2$, and the prefactor a obtained in a fit to the $T = 1.95$ data ($T_c = 2.203(1)$). The other curves are drawn using the same value of a .

E. Numerical results for the initial cross-over

The relationship $\phi_q \approx L^p t^{\nu(p-y_q)}$, which is a reduced form of Eq. (11) for $tL^{1/\nu'_q} \rightarrow 0$ and applicable to the development of discrete order, has not been tested directly in numerics (though the consequences were probed in Ref. [38] by analyzing data in other ways). Here, we present data from Monte Carlo simulations of the $q = 6$ hard clock model with $J = 1$ and temperatures chosen to be slightly below $T_c = 2.203(1)$. Our method for determining the critical point in all cases is through Binder cumulant crossing points [45, 46], as discussed in Appendix B.

Fig. 2 shows a common fit to data for ϕ_6 versus L for four different choices of $T < T_c$ and using $p = 2$ to test the consistency with the expected form. We used the best known value of the scaling irrelevant dimension, $y_6 = -2.509 \pm 0.007$ [36]. We fixed the prefactor of the power law at $T = 1.95$ and used the same factor for all other temperatures, together with the predicted scaling factor $t^{\nu(p-y_q)}$ for the different values of t . The consistency of the fit with the data seen in Fig. 2 is strong evidence that the functional form predicted by Eq. (11) is accurate. For all the models studied in this manuscript, T_c (and the quantum equivalent s_c) is extracted using the method of extrapolation of This is explained in detail in App. B, along with a table listing all the values of T_c extracted for the isotropic and anisotropic classical clock model.

III. EFFECT OF ANISOTROPY

As the purpose of this manuscript is to study the 2D quantum analogue of the 3D classical hard clock model, we first review the mapping between these two cases using the Suzuki-Trotter formalism in Sec. III A, and

present a discussion of numerical results in Sec. III B. This is followed by a phenomenological argument in Sec. III C for the observed $p = 3$ behavior.

A. Quantum to Classical Mapping

The mapping is carried out using a transfer matrix representation of the partition function $Z = \text{Tr}[\exp(-\beta H)]$. We can construct a quantum clock model in 2D using a Hamiltonian of the form $H = V + K$, where V is diagonal in the basis of clock degrees of freedom and encodes the $\cos(\theta_i - \theta_j)$ constraint in the spatial dimensions. K acts as the kinetic term generating quantum fluctuations and has off-diagonal matrix elements. For non-trivial quantum behavior, $[V, K] \neq 0$, and the Suzuki-Trotter expansion allows us to approximate the partition function using

$$e^{-\beta(V+K)} = \lim_{n \rightarrow \infty} (e^{-\frac{\beta}{n}V} e^{-\frac{\beta}{n}K})^n. \quad (14)$$

Using $\beta = n\Delta\tau$, it can be shown that this expression leads to an approximation of $O(\Delta\tau^2)$ [47]. As we are concerned with the ground state behavior of this system, we take $\beta \propto L$, as the gap is expected to scale with inverse linear size for a conventional quantum critical point with dynamic exponent $z = 1$.

The expansion of the partition function described above can be connected to the same for a 3D classical clock model written in terms of transfer matrices T . First we choose two directions to act as the classical dimensions of the quantum model and write the classical partition function as $Z = \text{Tr}[T^L]$, where the direction corresponding to imaginary time has L slices to simulate $\beta \propto L$. We decompose T into $V_c K_c$, which are the classical equivalents of the in-plane (ip) and out-of-plane (op) weights. Similar to the quantum case, each of these is a $q^{L^2} \times q^{L^2}$ matrix. V_c is diagonal and has matrix elements given by

$$[V_c]_{ii} = e^{-\beta_c H_{c(ip)}(C_i)}, \quad (15)$$

where β_c is the inverse temperature of the classical model and C_i corresponds to the configuration i of the spins in the plane. The correspondence to the quantum case requires us to choose $V_c = \exp(-\Delta\tau V)$, and as V_c and V are both diagonal, this is easily done using the matrix property that the exponential of a diagonal matrix is a diagonal matrix where the individual elements have been exponentiated. As $\Delta\tau \ll 1$,

$$H_{c(ip)} = - \sum_{\langle i,j \rangle} J_s \cos(\theta_i - \theta_j) \quad (16)$$

must have a $J_s \ll 1$ associated with it. This correspondence is more involved for the terms in the imaginary time direction, K_c and K . K_c is an off-diagonal matrix with elements given by $[K_c]_{i,j} = \exp(-\beta_c H_{c(op)}(C_i, C_j))$. Similar to the in-plane Hamiltonian, we can assign

$$H_{c(op)} = - \sum_{\langle i,j \rangle} J_t \cos(\theta_i - \theta_j). \quad (17)$$

To make a direct comparison to $\exp(-\Delta\tau K)$, we first normalize $[K_c]_{i,i} = 1$ for all i (this can always be done as this term does not have any in-plane, i.e. configuration specific terms). Then we use $\Delta\tau \ll 1$ to expand $\exp(-\Delta\tau K)$ as $1 - \Delta\tau K$. Assuming that K only has off-diagonal terms as it encodes quantum fluctuations, this can now be compared to K_c . As the terms in the imaginary time direction do not produce correlations across spatial sites, i.e. the bonds exist only between the same spin on different layers and not between spins at different sites, we need to consider only a reduced form of K_c or K which is a $q \times q$ matrix. Terms in K_c of the form $[K_c]_{i,i+1} = \exp(\beta_c J_t (\cos(2\pi/q) - 1))$ should now be compared with $\Delta\tau K_{i,i+1}$, forcing $J_t \rightarrow \infty$. This construction implies that the terms of the form $[K_c]_{i,i+2}$ are ignored as they are much smaller than $[K_c]_{i,i+1}$. The above analysis leads us to conclude that the quantum model is well described by an anisotropic clock model with $J_t \gg J_s$.

A modification of the imaginary time Hamiltonian for the classical case is to assume a Potts like interaction, given by $\delta_{\theta_i, \theta_j}$. This then simplifies the treatment of $[K_c]_{i,j}$ as all off-diagonal terms are equal. Choosing K to also be Potts like makes the analogy exact at $O(\Delta\tau^2)$. We study both forms of anisotropy in this section.

B. Numerical Results for the Anisotropic Clock Model

Following the analysis developed above, we define an anisotropic hard clock model on a cubic system of linear size L , with the following Hamiltonian:

$$H = -J_s \sum_{\langle i,j \rangle_s} \cos(\theta_i - \theta_j) - J_t \sum_{\langle i,j \rangle_t} \cos(\theta_i - \theta_j), \quad (18)$$

where $s(t)$ denotes bonds in directions corresponding to space (imaginary time). As the quantum model is expected to correspond to $J_t \gg J_s$, we define both coupling constants using the anisotropy $a \in [0, 1]$ as $J_t = 1 + a$ and $J_s = 1 - a$. As the behavior is not expected to be specific to extreme anisotropy, we examine a range of a to verify that qualitatively the behavior is similar to that of the isotropic case $a = 0$. Studies such as these have been carried out numerically for the Ising model [48], where it was found that the low energy universal physics at the phase transition is not affected by the strength of the anisotropy. Note that even though we consider the quantum model to correspond to the extreme anisotropy limit, from a continuum field theory perspective, this would not be the case as a finite velocity is expected in space time.

We first study the Monte Carlo flow diagram and find that it is similar to the isotropic case [38]. This suggests that we still have behavior controlled by the 3D XY fixed point at criticality. The growth of the U(1) breaking order parameter ϕ_6 can also be studied now as the flow deviates from the NG fixed point, similar to the treatment presented in the previous section. For $a = 0.5$, we find that for relatively large $t = T_c - T$, we get behavior

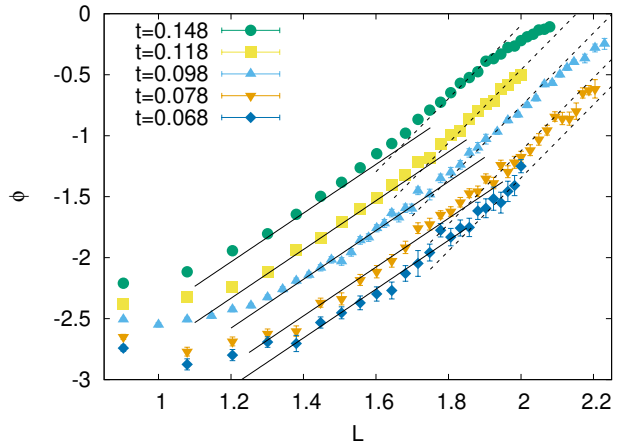


FIG. 3. Scaling of ϕ_6 as a function of system size for the anisotropic clock model with $a = 0.5$, shown on a log-log scale. A fit to $f(x) = a_p L^p t^{\nu(p-yq)}$ for $p = 2$ and 3 is performed only for $t = 0.098$ for appropriate size ranges, and the functions are plotted for all values of t .

consistent with $\phi_6 \propto L^2$, but at smaller t , we find that the flow can be clearly separated into regions dominated by L^2 and L^3 . This is clearly seen in Fig. 3, where the L^2 fit works well for small ϕ_6 and L^3 for intermediate values up to unity. This implies that the argument presented in the previous section relating the transverse susceptibility of the goldstone mode to the value of $p = 2$ is still valid, as would be expected for the long wavelength physics. It is important to note here that Eq. (12) automatically sets the exponent for t once a value of p is chosen. This implies that individual fits need not be performed for various t . This is the technique we use in Fig. 3, where the central data set ($t = 0.098$) is used to extract the overall proportionality constants $c_2(c_3)$ for $p = 2(3)$, and the fits are applied to all data sets. This strengthens the conclusion that Eq. (12) predicts the L and t dependence.

The $p = 3$ behavior is found to be strengthened at $a = 0.9$, where the L^2 range is almost unidentifiable. Fig. 4 shows this for an order of magnitude range in system size and small values of ϕ_6 . As discussed previously in this section, it is also important here to consider other forms of anisotropy as the quantum to classical mapping does not create exactly the same term in the imaginary time direction as the anisotropic clock model considered here. The Potts like interaction is therefore of special importance, as it can be copied faithfully into the quantum case. This corresponds to the imaginary time interaction in the anisotropic clock model to be modified to

$$-J_t \sum_{\langle i,j \rangle_t} \delta_{\theta_i, \theta_j}. \quad (19)$$

We have studied the scaling of ϕ_6 close to the NG fixed point. This is also shown in Fig. 4 for $a = 0.9$ and we clearly see an L^3 dependence. These results suggest that the L^3 behavior is robust to some extent to the kind of interaction used in the imaginary time direction.

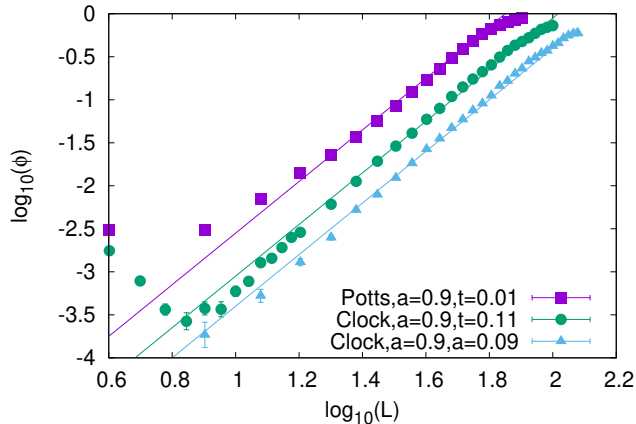


FIG. 4. Scaling of ϕ_6 as a function of system size for the anisotropic clock model with $a = 0.9$, shown on a log-log scale. Also shown is the same for the clock model with Potts-like interaction in the imaginary time direction with $a = 0.9$. Fits are to $f(x) = aL^3$.

We also use another technique to directly identify the critical exponent ν'_6 using the relation given in Eq. (2), and exponents already known in the literature. We present this approach here for $a = 0.95$ and use it in the next section to analyze the quantum models. For our analysis, we use $\nu = 0.6717(1)$ for the 3D XY model [44] and $y_{q=6} = -2.509(7)$ for the classical clock model [43]. Using $p = 3$ and Eq. (2), we have $\nu'_6 = 1.234(1)$; from this point on, and for all the captions of the figures, we will call this value α_3 . The corresponding value for $p = 2$ is denoted by $\alpha_2 = 1.514(1)$. We can verify Eq. (2) by studying the region of the flow diagram where $\phi_q \approx O(1)$. When $\phi_q \rightarrow 1$, Eq. (12) can be reduced to

$$\phi_q = 1 - k(tL^{1/\nu'_q}). \quad (20)$$

Now one can pick a constant c , which sets a horizontal cut $\phi_q = c$, in the flow diagram. Taylor expanding Eq. (20) about $\phi_q = b$ such that $b \approx c$, leads to $c = b + \alpha t L_c^{1/\nu'_q}$, which can be inverted to a leading behavior of $L_c \approx t^{-\nu'_q}$. This length, $L_c(t)$, can be extracted for a range of t and c , to test this scaling law. This has been checked for the classical 3D clock model [38], and ν'_q found to be scaling consistent with $p = 2$. We check the same for strong anisotropy ($a = 0.95$) and find fits to both α_3 and α_2 in different ranges of t . This is shown in Fig. 5, where (a) shows the variation of ϕ_q with size for various values of L , and the (b) shows the intercepts L_c extracted using $\phi_q = 0.2$ and 0.4 . This dual power law behavior is not accessible for weaker anisotropy due to limitations on computational power, as the cross-over occurs at larger sizes with decreasing anisotropy. For any non-zero anisotropy, the asymptotic behavior at arbitrarily small t should correspond to $p = 3$. Due to the arguments presented in the previous section and App. A, we expect that the isotropic case shows a behavior con-

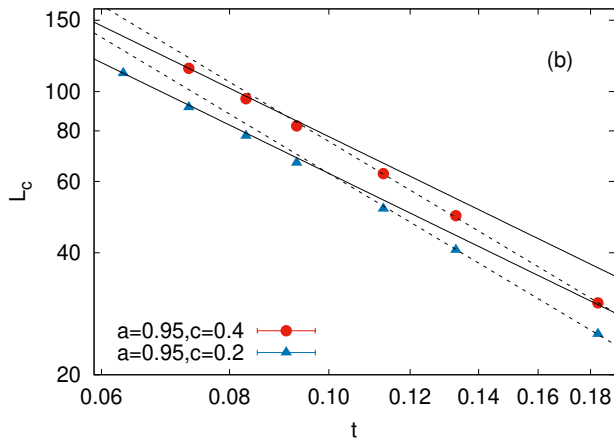
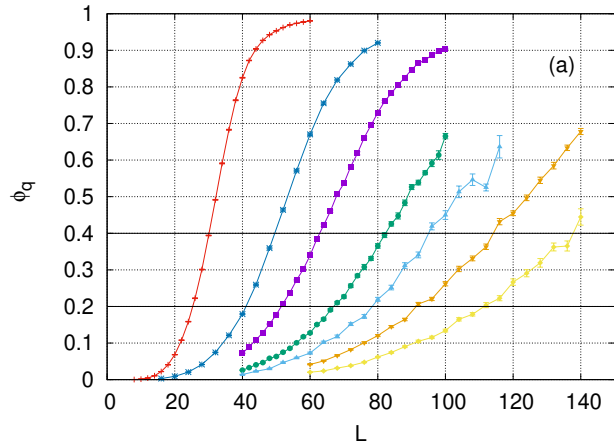


FIG. 5. (a) ϕ_q as function of linear size L for $q=6$ and values of t ranging from $t = 0.063$ to $t = 0.183$. (b) Corresponding L_c as a function of t for various cuts $\phi_q = c$, fit to the form $L_c = at^{-\alpha_3}$ for only the smallest value of t and $L_c = at^{-\alpha_2}$ for high t (Anisotropy parameter $a = 0.95$).

sistent with α_2 for arbitrarily small t .

C. Phenomenological Justification for $p = 3$

The exponent ν'_q associated with $p = 3$ has been predicted to be generated by considering the effects of a finite ξ on a large system size. In this limit, the system can be considered as being made up of cubic blocks of linear size ξ . The scaling variable for the free energy is controlled by the number of such cubes, which scales as L^3 . As this intuition was first developed for the isotropic case [31], and is not supported by numerics [38], we expect that this description does not capture the lowest energy excitations present in the system. Numerous studies of excitations in the 3D XY model [40, 49, 50] have shown that the dominant fluctuations are of the form of vortex loops. As the region of the flow diagram which we are investigating here is primarily of an XY nature close to the NG fixed point [38], it would be reasonable to ex-

pect that these vortex loops would play a major role. A detailed study [40] of the anisotropic XY model in 3D, shows that the vortex loops get elongated along the direction of strongest anisotropy. This lends support to the idea that topological vortex line defects which span the entire system may be present. Further support is given to this idea by experimental [51] and numerical [52] studies of ferroelectrics, which are modeled by anisotropic 6-state clock models. These studies have found that annealing through the critical point leads to frozen defects which are consistent with vortex lines. We conjecture that the $p = 3$ behavior is a result of discrete symmetry breaking in the presence of vortex line defects, following the analysis at the end of the previous section. It is important to note here that a vortex flux line description would be consistent with our observation that the exact form of the interaction used in the imaginary time direction does not play a role in determining the universal behavior.

The effects of anisotropy on Eq. (13) can also be studied using a renormalization group picture of vortex loops. It has been shown [40] that vortex loop excitations are elongated in the direction of strong anisotropy and are renormalized to the isotropic point with increasing length scales. We have incorporated the arguments of Ref. [40] in App. A and show that the form of the transverse susceptibility in Eq. (13) remains the same in the asymptotic limit. This implies that to get a $p = 3$ dependence in Eq. (2), we must modify the relationship between \bar{h} and the bare field anisotropy h . In the isotropic case, we expect that the renormalization of the $\cos(q\theta)$ irrelevant operator under a scale change of $a \rightarrow ba$, where a is the lattice spacing, leads to $h \rightarrow b^{y_q}h$. In the anisotropic case, if we assume that the renormalization affects only the spatial directions, then a scale renormalization for a 3D system leads to $h \rightarrow (b^{y_q})^{2/3}h$, due to a scaling dependence on the third direction which is either absent or slow compared to the spatial one. If we use this expression in our analysis of Eq. (13), we get a modification of the relation between the physical k and h , leading to $k\xi \approx \xi^{y_q/3}$. Using this and the substitutions for ν and ν'_q as in the isotropic case, we recover the equivalence expressed in Eq. (2) with $p = 3$.

IV. QUANTUM CLOCK MODEL

As discussed in the previous section, the form of the quantum fluctuations for the hard clock model in 2D allows for some flexibility. The general model we use is described by the Hamiltonian:

$$H = -s \sum_{\langle i,j \rangle} \cos(\theta_i - \theta_j) - (1-s) \sum_i T_i^x, \quad (21)$$

where T_i^x acts as a quantum fluctuation acting only on site i . We test three simple choices for this fluctuation to show that our results are robust to the exact form. These choices are:

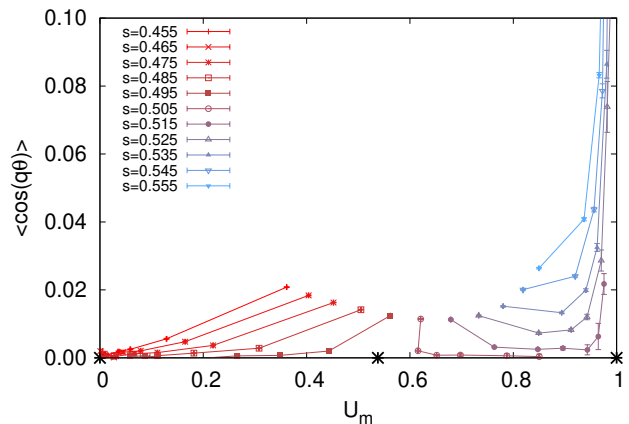


FIG. 6. Flow diagram for $q = 6$ (ϕ_q vs U_m) and for choice (2) showing flows (critical flow at $s_c = 0.50149(6)$) approaching the XY fixed point followed by the Z_q fixed point. The stable disordered point (0,0) is marked here along with the unstable XY (0.532,0) and NG (1,0) points.

- 1) $\langle \theta_i | T_i^x | \theta'_i \rangle = \cos(\theta_i - \theta'_i) + 1$ only for $\theta_i - \theta'_i = 2\pi/q$ and zero otherwise. This choice is most clock-like as it allows only transitions to the directions one step away from the current direction.
- 2) $\langle \theta_i | T_i^x | \theta'_i \rangle = \cos(\theta_i - \theta'_i) + 1$ with no constraint. This choice also provides clock-like fluctuations as it provides lesser weight to large changes in direction.
- 3) $\langle \theta_i | T_i^x | \theta'_i \rangle = 1/q$ with no constraint. This choice is a Potts-like interaction in the imaginary time direction and provides no notion of the 2D form of the degree of freedom.

We simulate the three models mentioned above using stochastic series (SSE) expansion quantum Monte Carlo (QMC) [53] for the transverse field Ising model (TFIM), as it is a powerful and unbiased method of extracting thermodynamic expectation values for such systems. The algorithm for quantum clock models follows closely that for the TFIM, along with modifications to the cluster algorithm to improve efficiency. We extract the critical point in all three cases using the Binder cumulant of the magnetization as

$$U_m = \left(2 - \frac{\langle M^4 \rangle}{\langle M^2 \rangle^2} \right); \quad \vec{M} = \frac{1}{N} \sum_{i \in S} \vec{M}_i, \quad (22)$$

where S corresponds to all N spins in the square lattice. We find that the critical behavior matches the 3D XY fixed point. Once again the $U(1)$ breaking order parameter is given by $\phi_q = \langle \cos(q\theta) \rangle$, where θ is now defined using the \vec{M} as defined above. Evidence for the 3D XY critical behavior is shown in Fig. 6, in the form of the Monte Carlo flow diagram for choice (2). The scaling dimension of the dangerously irrelevant operator are shown

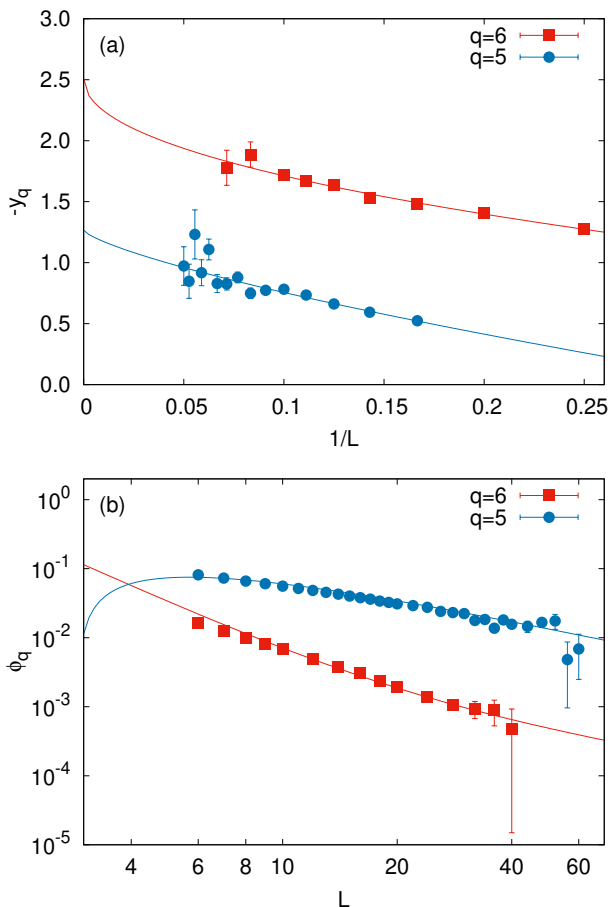


FIG. 7. (a) $-y_q$ calculated using the Binder cumulant crossing method as a function of $1/L$. Fit to $f(x) = a/L^b + c$ where c is fixed to the scaling dimensions provided in Ref. [43]. (b) ϕ_q as a function of system size at the critical point, fit to power laws for $q = 5, 6$ using the same scaling dimensions as (a) along with a correction of the form a/L^b . These plots correspond to choice (3).

for choice (3) in Fig. 7 for $q = 5, 6$. This choice is presented as we were able to get the highest quality data for the finite size scaling for this choice. The critical exponents are consistent with the known values at the 3D XY point [43, 44], and numerical evidence for this is shown in Appendix B. The decay of ϕ_q at the critical point is also shown explicitly in Fig. 7, using the exponents provided in Ref. [43].

This establishes that the critical behavior is indeed 3D XY like, and that a scaling analysis of ϕ_6 can be carried out in the vicinity of the NG point. We check the hypothesis that $\phi_q \propto L^p$ using two different definitions of the U(1) breaking order parameter, for choices (1) and (2). The first, and the one we have used above for the flow diagram and scaling analysis, is denoted by $\phi_q^{(2)}$, uses only spins in the plane to define θ as shown in Eq. (22), and the second, denoted by $\phi_q^{(3)}$, uses all the spins in space

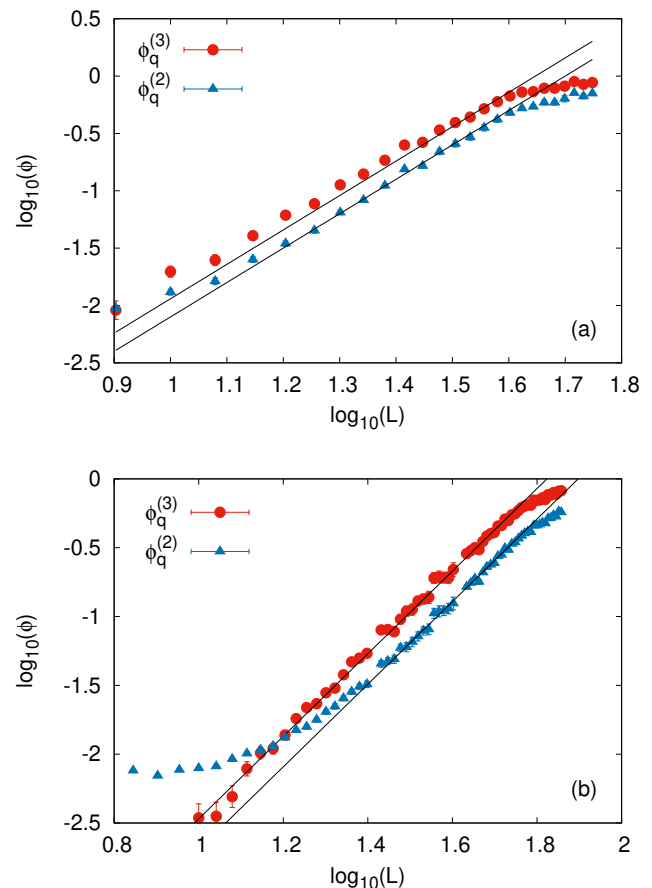


FIG. 8. 2 and 3 dimensional versions of ϕ_q fit to aL^3 in relevant size ranges for (a) choice (1) with $(s - s_c) = 0.05955$ and (b) choice (2) with $(s - s_c) = 0.0245$ and $q = 6$.

time to define the same as

$$\vec{M} = \frac{1}{NL_\tau} \sum_{i \in V} \vec{M}_i, \quad (23)$$

where V corresponds to the entire 3D space-time volume, and L_τ corresponds to the extent of imaginary time. L_τ is taken to be large enough to ensure convergence to the ground state. We expect $p = 3$ for the flow away from the NG point from our study of the anisotropic classical clock model. This should be valid as long as $\phi_q \ll 1$. We set $q = 6$ and choose a value of $(s - s_c)$ such that it allows a large range of sizes, and the intermediate sizes are fit to aL^3 . The results are shown for choice (1) in Fig. 8a with $(s - s_c) = 0.05955$, and we see consistency with the fit. A similar analysis for choice (2) is also shown in Fig. 8b for $(s - s_c) = 0.0245$.

We can once again use the technique of the size intercept described in the previous section to get a reliable estimate for the value of ν'_q . We first present this approach for choice (2). For our analysis, we use α_2 and α_3 as defined for the classical clock model in Sec. III B. All of our results from this point on are for the $q = 6$

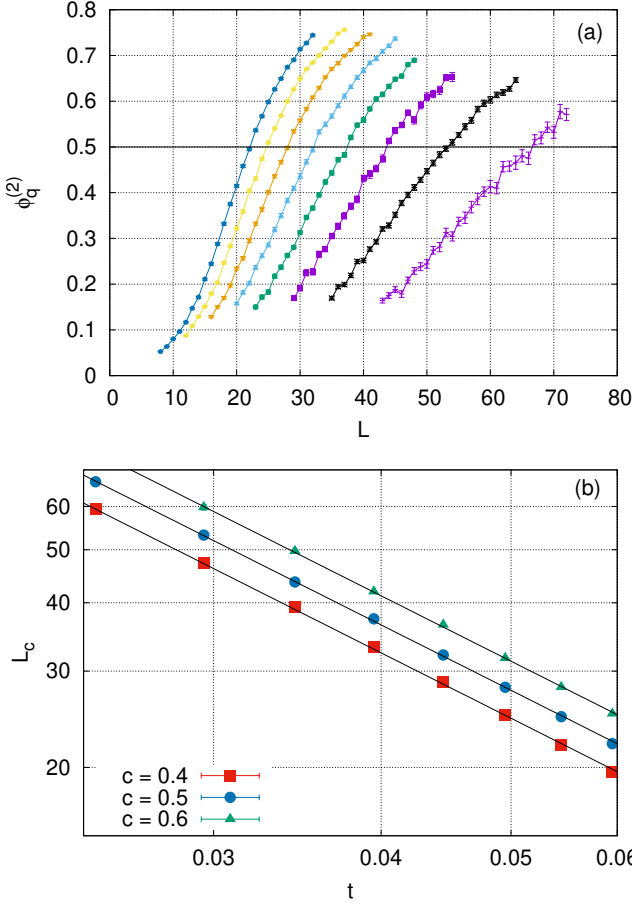


FIG. 9. (a) $\phi_q^{(2)}$ as function of linear size L for $q=6$ and values of t ranging from $t = 0.0595$ to $t = 0.0245$. (b) Corresponding L_c as a function of t for various cuts $\phi_q^{(2)} = c$, fit to the form $L_c = at^{-\alpha_3}$. These plots are for choice (2).

quantum clock model.

Following the technique described in Sec. III B, we can construct plots similar to Fig. 5, for the quantum case. We check this for both the 2D ($\phi_q^{(2)}$) and the 3D definition ($\phi_q^{(3)}$) of the U(1) breaking order parameter, which would be expected to have the same scaling.

We show the extraction of L_c from $\phi_q^{(2)}$ as a function of t in Fig. 9 for choice (2) and $c = 0.4, 0.5, 0.6$. We plot the extracted (L_c, t) points on a log-log plot and fit a power law consistent with $\nu'_q(p=3)$. The same analysis is carried out for $\phi_q^{(3)}$ and choice (2) in Fig. 10, and once again we find behavior consistent with $\nu'_q(p=3)$.

To confirm that this behavior is truly isotropic in space time, we also check the same using line definitions of the U(1) order parameter.

The spatial line order parameter is defined by calculating the magnetization \vec{M} for a row on the square lattice, and defining θ using this vector. The temporal line order parameter is calculated by doing the same for a column in imaginary time associated with a particular

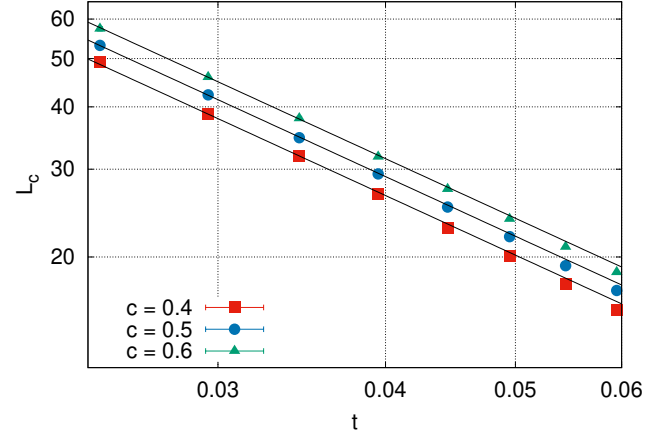


FIG. 10. L_c as a function of t for various cuts $\phi_q^{(3)} = c$, fit to the form $L_c = at^{-\alpha_3}$. This plot corresponds to choice (2) and $q = 6$.

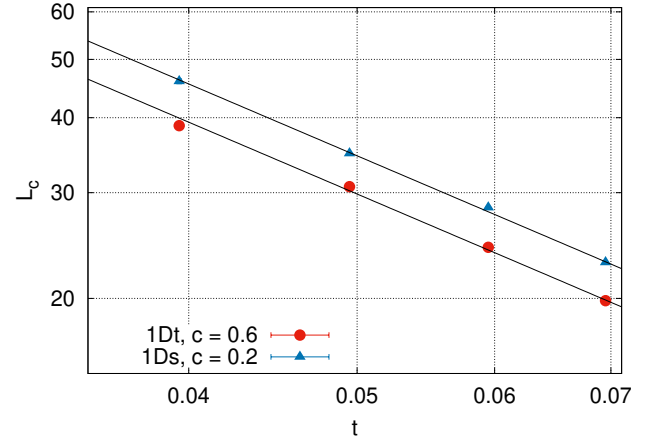


FIG. 11. Line order parameters (spatial and along imaginary time) used to calculate ν'_6 , fit to the form $L_c = at^{-\alpha_3}$, for choice (2) and $q = 6$.

spatial site. Translational invariance is used to average these quantities across space-time. We find the same behavior for these order parameters as well, as shown in Fig. 11; where the line imaginary time order parameter, labeled by “1Dt”, is calculated at an intercept value of $c = 0.6$, whereas the line spatial order parameter, labeled by “1Ds”, is calculated at an intercept value of $c = 0.2$. We choose the largest possible value of c for which the size L_c can be consistently calculated using the data available. This helps us probe the largest sizes and reduce finite size effects.

Now we turn to choice (3) and carry out the same analysis. The scaling analysis for ν'_q also yields the same exponent as the more conventional quantum clock models discussed above (Figs. 12). This leads to the conclusion that this feature is independent of the particular form of the quantum fluctuation. The study of the different

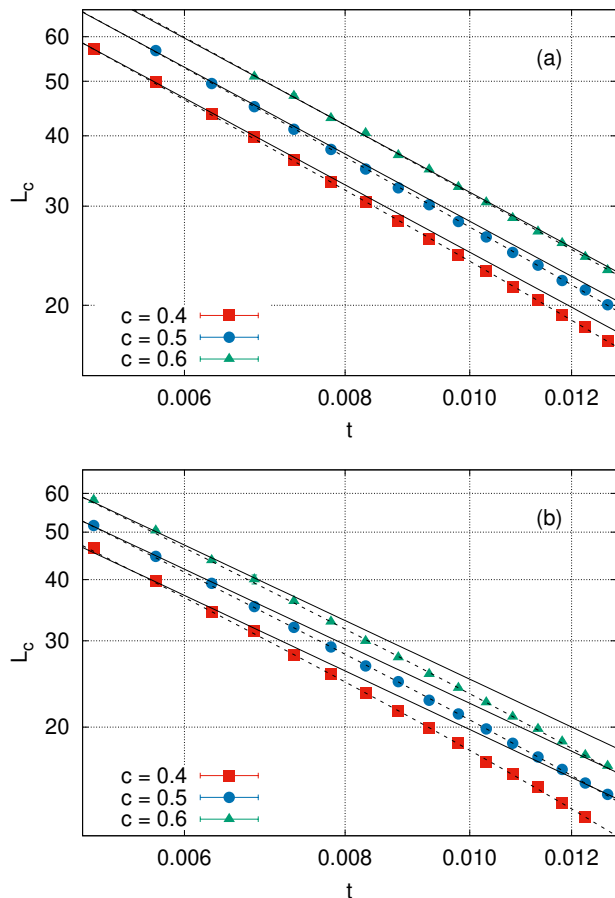


FIG. 12. L_c as a function of t for various cuts for (a) $\phi_q^{(2)} = c$ and (b) $\phi_q^{(3)} = c$, fit to the form $L_c = at^{-\alpha_3} + b$, for choice (3) and $q = 6$.

definitions of the order parameter to detect the discrete symmetry breaking leads to a single correlation length exponent. This implies that the behavior is isotropic in space time.

A comparison to the results of the anisotropic clock model in the previous section shows us that for the quantum clock models which we have studied, behavior consistent with $p = 2$ is not seen for the large range of sizes which we have studied. This implies that the quantum case corresponds to large anisotropy in the language of the 3D clock model.

V. DOMAIN WALLS

One of the most direct probes of the two length scales is the domain wall energy. It was predicted[41] and found numerically[12] that the domain wall energy density for a system with two length scales ξ and ξ' (where $\xi' \gg \xi$) has a dependence on both terms. The domain wall width is expected to be controlled by the larger length scale ξ' , while the free energy density, which would gener-

ically have a dependence on both scales, is expected to be dominated by the smaller length scale ξ through $\Delta F \propto \xi^{-(d+z)}$. Taking both of these arguments into account along with a universal function $Y(\xi/L, \xi'/L)$ for the scale invariant part of the free energy, and following the arguments shown in the supplemental material of Ref. [12], the domain wall energy density, defined as the excess free energy per unit area of the domain wall, reduces to

$$\Delta E \approx (\xi^{d+z-2} \xi')^{-1}. \quad (24)$$

As we are considering 2+1D quantum or 3D classical models, we use $d + z - 2 = 1$. The second length scale considered here can correspond to either a dangerously irrelevant operator[35] in general or the size of a deconfined spinon in the particular case of deconfined quantum criticality. To check the validity of the above expression using finite size scaling, one can replace both ξ and ξ' by the system size L . For the case we are studying here, that would imply $\Delta E \approx L^{-2}$, and this has been verified for the classical 3D clock model[12]. This implies that both length scales are independently tuned by t . However, at the DQC point the length scale ξ' , which is associated with the deconfined spinon, saturates to system size for a finite system while the conventional diverging correlation length saturates at $\xi \propto L^{\nu/\nu'}$ with $\nu/\nu' < 1$. This leads to ΔE scaling as $L^{1+\nu/\nu'}$ [12]. These observations motivate us to use the domain wall energy to investigate the dependencies of the length scales for the quantum clock models.

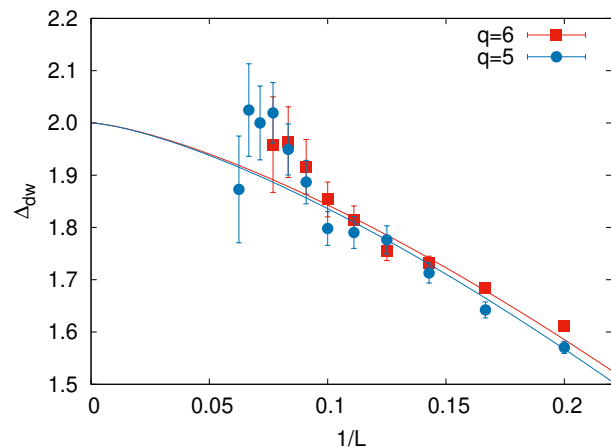


FIG. 13. Δ_{dw} calculated using the ratio of domain wall energies for pairs of sizes $(L, 2L)$ for varying L for choice (3). We fix $\Delta_{dw}(\infty) = 2$ for $q = 5, 6$ and fit the finite size data using a correction of the form a/L^b .

The domain wall energy is calculated by applying open boundary conditions on the 2D lattice which are inconsistent with the ordered state and measuring the excess energy over the ground state with consistent boundary conditions. The corresponding density is achieved by

normalizing this by the length in the unfrustrated direction. This quantity is determined using QMC simulations carried out at the critical point, where the correlation lengths begin to diverge and we can extract the scaling exponent from finite size scaling. For the quantum clock model, ideally we would like to investigate boundary conditions with a minimum twist, but as the domain wall energy is a small difference between energies which scale with system volume, and has strong relative fluctuations, we use maximum twist conditions. To this end, we fixed all $\theta_i = 0$ on the left boundary and all $\theta_i = \pi(4\pi/5)$ on the right boundary while maintaining periodic boundary conditions for the top and bottom boundaries, leading to a maximum twist for $q = 6(5)$. The scaling of the excess energy is found to be consistent with $\Delta_{dw} = 2$ for $q = 5$ and 6 , as seen in Fig. 13. This is consistent with the conventional finite-size scaling at a continuous phase transition that suggests that both ξ and ξ' must be replaced with L , leading to an exponent of 2.

VI. CONCLUSIONS

We have studied a 2D quantum clock model and explored the behavior of the length scale associated with U(1) symmetry breaking. We find that although the critical behavior remains in the 3D XY universality class, as expected from the isotropic classical clock model in 3D, the exponent ν'_q differs from that of the classical model. To motivate the development of this difference, we have studied an anisotropic classical clock model in 3D, and shown that at large values of the anisotropy, we recover the quantum behavior in a certain range of parameter space. We have also shown that this behavior is robust to the precise form of interaction applied in the imaginary time direction, and that the same behavior can be seen for a Potts-like interaction. Based on this observation and a phenomenological treatment presented in Sec. III, we conjecture that the anomalous behavior for the anisotropic clock model is a consequence of an anisotropic scaling associated with the irrelevant U(1) operator, where the spatial directions allow a renormalization of the coefficient associated with the operator and there is effectively no scaling in the imaginary time direction. We also suggest connections to vortex line excitations which are expected to be independent of the details of the imaginary time interaction, which is consistent with our findings. It would be worth setting our phenomenological understanding on stronger theoretical foundations based on renormalization group analysis, and we invite future collaborations on this.

These results have broad consequences for the large variety of 2D quantum and 3D anisotropic classical models which have discrete symmetries similar to the clock model. A special case of this is the valence bond solid formation in 2D quantum magnets, where the lattice forces a discrete symmetry breaking leading to behavior analogous to that studied here. An example of this is the

JQ model, which has been discussed in the introduction, and we would like to study this in detail in the future to study similar effects which anisotropy may have in that case as well.

Future directions also include a study of the quantum dimer model close to Rokhsar-Kivelson point, where emergent U(1) behavior is seen and development of discrete order can be expected on the ordered side of the transition. Another promising route to further our understanding of the development of discrete order in the clock model is to study the 2D classical clock model in the presence of disorder. The clean 2D classical model shows a KT phase separating the ordered and disordered phases [54], and the introduction of disorder is expected to shrink this phase and eventually lead to an infinite disorder fixed point separating the ordered and disordered phases [55, 56], leading to a vanishing of the U(1) symmetric phase, similar in spirit to the 3D case. Some signatures of the infinite disorder fixed point have been seen in numerical simulations of the disordered XY model [57].

ACKNOWLEDGMENTS

We would like to thank Deepak Dhar and Rajesh Narayanan for useful discussions. This work was supported by the NSF under Grant No. DMR-1710170 and by a Simons Investigator Grant. The computational work was performed using the Shared Computing Cluster administered by Boston University's Research Computing Services. PP would like to thank Institute of Physics, Chinese Academy of Sciences for hosting a fruitful visit and facilitating collaboration.

Appendix A: Transverse susceptibility of isotropic 3D XY model

Here we provide a short justification for the expression used for the transverse susceptibility in Eq. (13). Assume a 3D XY model at a temperature T slightly lower than T_c . As we want to ultimately study the clock model, we add a field $h \cos(q\theta)$. To minimize this, we assume that the XY ordering lies along $\theta = 0$ without loss of generality. We use a coarse grain description of the XY model by defining a continuous complex valued field ϕ , and a corresponding action given by

$$S = \int d^3x [\partial^\mu \phi \partial_\mu \phi^* - m\phi\phi^* + m_4(\phi\phi^*)(\phi\phi^*) - h(\phi^q + \phi^{*q}) - h_x(\vec{r}) \frac{1}{2i}(\phi - \phi^*)], \quad (\text{A1})$$

where the last term is added in to reflect a spatially varying transverse magnetic field of magnitude h_x , and the implied clock model is q -fold symmetric. First, we consider the above action for $h_x(\vec{r}) = 0$, and assume that we are solving simply for the configuration which minimizes the action and ignore fluctuations. This minimum would

be given by $\phi(\vec{r}) = A$, where A depends on $\{m, m_4, h\}$. Because we will be considering only small transverse fluctuations in $\phi(\vec{r})$, we can absorb A into the definitions of $\{m, m_4, h\}$ and set the configuration (to be reference state from now on) to be $\phi(\vec{r}) = 1$. As we want to study the infinitesimal transverse susceptibility, we now consider Eq. (A1) for $h_x(\vec{r}) = h_x \cos(kx)$, where x is along a randomly chosen direction as the system is isotropic. We can assume that the dominant response of the system would also be in the same Fourier component, implying that it should be magnitude preserving and of the form $\phi(\vec{r}) = \exp(ia \cos(kx))$, where $a \ll 1$. Using this expression for the field in Eq. (A1) gives us

$$S = \int d^3x [a^2 k^2 \sin^2(kx) - m - m_4 - h(2 - q^2 a^2 \cos^2(kx)) - h_x \cos(kx) a \cos(kx)], \quad (\text{A2})$$

where we have expanded the exponentials where necessary and kept only terms up to a^2 . Performing the integral and assuming $\int d^3x \sin^2(kx) = \int d^3x \cos^2(kx) = C$, the a dependent part of the action now is

$$S = C(a^2 k^2 + h q^2 a^2 - h_x a). \quad (\text{A3})$$

As we are only interested in the qualitative behavior of the transverse susceptibility in terms of h and k , h can be redefined to absorb q^2 . The action above can now be minimized by setting $a = 0$ (unphysical solution) or $a = h_x / (k^2 + h)$. This result implies $\phi(\vec{r}) = 1 + i(h_x / (k^2 + h)) \cos(kx)$ for small a .

The transverse susceptibility at a particular position is defined as

$$\chi(\vec{r}) = \lim_{h_x \rightarrow 0} \frac{\phi(\vec{r})_{h_x} - \phi(\vec{r})_0}{h_x}. \quad (\text{A4})$$

The analysis presented above thus implies $\chi(\vec{r}) = (i / (k^2 + h)) \cos(kx)$. Taking the Fourier component of this at wave vector k leads to the expression presented in Eq. (13). It must be noted here that the variables k, h used here are the renormalized values and are equivalent to the \bar{k}, \bar{h} values in Eq. (13). Their relation to physical scales are discussed below Eq. (13).

We can extend this analysis to the limit of strong anisotropy, by incorporating renormalization group flows from Ref. [40]. Following their notation, we quantify the anisotropy using $\gamma_0^{-2} = J_\perp / J_\parallel$, where we are interested in bare couplings with $\gamma_0^{-2} \gg 1$. Eq.(C18) of Ref. [40] shows that γ_0^{-1} is irrelevant under RG flow and asymptotically approaches the fixed isotropic point $\gamma^{-1} = 1$. In the analysis following Eq.(C18), the authors show that the flowing value of the anisotropy at scale l is $\gamma_l^{-1} = 1 + ce^{-l}$, where $e^l = a_l / a_0$, and $a_l(a_0)$ corresponds to the renormalized(bare) length scale. As they also show that the renormalized isotropic interaction is $J_{iso} = \sqrt{J_\perp J_\parallel}$, the flowing forms of the interaction strengths can be written as $J_\perp^l = J_{iso}(1 + c \frac{a_0}{a_l})$ and $J_\parallel^l = J_{iso} / (1 + c \frac{a_0}{a_l})$.

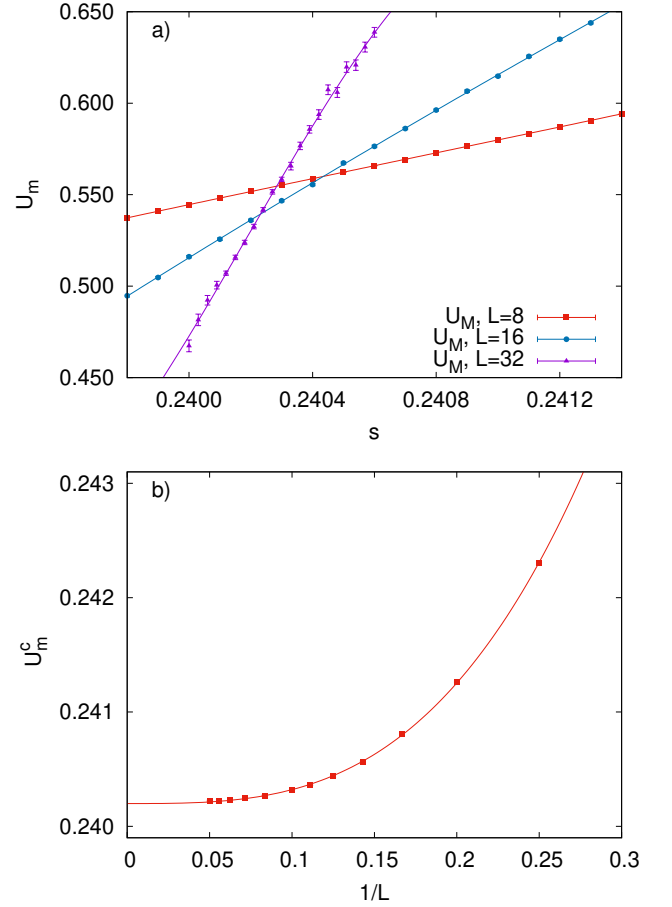


FIG. 14. (a) U_m for three sample sizes for the quantum clock model with Potts-like kinetic term, i.e, choice (3) of Sec. IV.(b) Crossing points of U_m , defined as U_m^c for sizes L and $2L$, extrapolated using $f(x) = s_c + a/L^b$ gives us $s_c = 0.240199(5)$.

The above analysis shows how the kinetic term in the action (Eq. (A1)) has to be modified to accommodate the anisotropy. As we are assuming that we are in the ordered phase of the clock model and at scales where it is safe to assume that the XY magnetization is ordered, one can ignore the dependence of m and m_4 on direction.

Coming back to Eq. (A1), we can now see that the form of the action differs depending on which direction we choose for our transverse field variation. We will label our axes as x, y, z , where z corresponds to imaginary time and x, y correspond to space. We first investigate the effect of an applied transverse field of $h_z(\vec{r}) = h_z \cos(kz)$. In addition to this, we set the scale of $J_{iso} = 1$, so that the coefficients in front of the kinetic term $\partial^z \phi \partial_z \phi$ is $(1 + c \frac{a_0}{a_l})$ and for x and y is $1 / (1 + c \frac{a_0}{a_l})$. As the transverse field is assumed to be varying only in z , the x and y kinetic terms are irrelevant. Once again, we assume a response of ϕ to be at the same wavelength as $h_z(\vec{r})$ and minimize the action as done earlier for the isotropic case. This

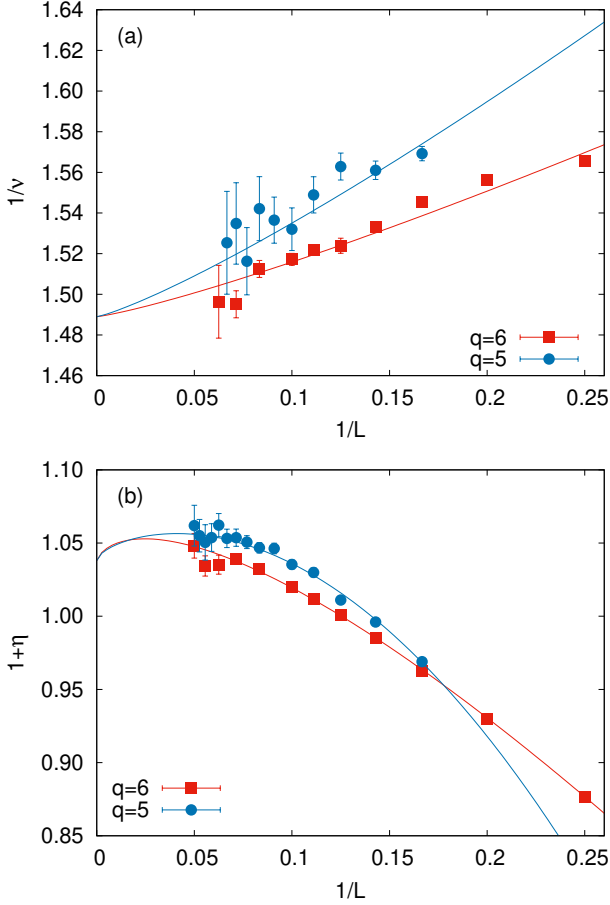


FIG. 15. (a) $1/\nu$ as a function of $1/L$ for choice (3), extrapolated using $f(L) = 1/\nu_\infty + a/L^b$, where ν_∞ is set to the known value for the 3D XY model. (b) $1 + \eta$ as a function of $1/L$ for choice (3), extrapolated using two corrections to capture non-monotonic behavior.

gives a final transverse susceptibility which goes as

$$f_\perp(k, h) = \frac{1}{(1 + c\frac{a_0}{a_t})k^2 + h}. \quad (\text{A5})$$

If we were to perform the same analysis using a transverse field which varied in the x -direction (x and y directions are equivalent), we would get a similar form for $f_\parallel(k, h)$, with the k -dependent part modified such that

$$f_\parallel(k, h) = \frac{1}{(1 + c\frac{a_0}{a_t})^{-1}k^2 + h}. \quad (\text{A6})$$

Note that for both of these forms of the transverse susceptibility, the asymptotic behavior for a crossover between h and k can still be considered to be controlled only by k^2 . In this way, other than non-universal behavior generated before the approach to the asymptotic limit, the transverse susceptibility is identical to that derived for the isotropic case.

Appendix B: Critical point and scaling dimension estimation using Binder cumulant crossing points

The critical values of the temperatures T_c for the classical models and the tuning parameters s_c for the quantum models are calculated using the crossing points of Binder cumulants U_m , as it shows a sharp transition between 0 and 1 at the critical point. This transition has an increasing gradient with increasing systems size, allowing us to define crossing points as shown in Fig. 14a. We extrapolate crossing points for sizes L and $2L$ as a function of $1/L$ to the infinite size limit. This is shown clearly in Fig. 14b for choice(3) of Sec. IV.

The critical values s_c for the three choices of quantum fluctuations which we have used in Sec. IV extracted using this technique are listed in the table below, along with the critical temperatures T_c for varying values of the anisotropy a for the anisotropic clock model discussed in Sec. III.

Quantum	s_c	Classical	T_c
choice 1	0.340450(7)	$a=0$	2.203(1)
choice 2	0.50149(6)	$a=0.50$	1.697(1)
choice 3	0.240199(5)	$a=0.90$	0.8945(2)
		$a=0.95$	0.683(2)

We have also calculated the critical exponents ν and η associated with the quantum phase transition for choice (3) of the quantum fluctuations. These are calculated for a particular size L by comparing the value of the relevant observables (slope of Binder cumulant for ν , and magnetization for η) at sizes L and $2L$ and at s given by the crossing points of U_m curves for the respective sizes. These values are shown in Fig. 15, along with an extrapolation to the infinite size limit for $q = 5, 6$ using the known values for the 3D XY model [44], which are $\nu = 0.6717(1)$ and $\eta = 0.0380(4)$. Using corrections which have a generic form of a/L^b , we are able to achieve reasonable fits. To have an acceptable fit for η in Fig. 15b, we need to use two correction terms which capture the non-monotonic behavior.

-
- [1] M. G. Yamada, M. Oshikawa, and G. Jackeli, Emergent SU(4) Symmetry in α -ZrCl₃ and Crystalline Spin-Orbital Liquids, Phys. Rev. Lett. **121**, 097201 (2018).
 [2] R. Coldea, D. A. Tennant, E. M. Wheeler, E. Wawrzynska, D. Prabhakaran, M. Telling, K. Habicht, P. Smeibidl, K. Kiefer, Quantum criticality in an Ising chain: experi-

- mental evidence for emergent E8 symmetry, Science **327**, 5962 (2010).
 [3] J. Schmalian and C. D. Batista, Emergent symmetry and dimensional reduction at a quantum critical point, Phys. Rev. B **77**, 094406 (2008).
 [4] T. Schulz, R. Ritz, A. Bauer, M. Halder, M. Wagner,

- C. Franz, C. Pfeleiderer, K. Everschor, M. Garst and A. Rosch, Emergent electrodynamics of skyrmions in a chiral magnet, *Nature Physics* **8**, 301 (2012).
- [5] T. Senthil, A. Vishwanath, L. Balents, S. Sachdev and M. P. A. Fisher, Deconfined quantum critical points, *Science* **303**, 1490 (2004).
- [6] M. Levin and T. Senthil, Deconfined quantum criticality and Néel order via dimer disorder, *Phys. Rev. B* **70**, 220403 (2004).
- [7] A. W. Sandvik, Evidence for Deconfined Quantum Criticality in a Two-Dimensional Heisenberg Model with Four-Spin Interactions, *Phys. Rev. Lett.* **98**, 227202 (2007).
- [8] J. Lou, A. W. Sandvik, and N. Kawashima, Antiferromagnetic to valence-bond-solid transitions in two-dimensional SU(N) Heisenberg models with multispin interactions, *Phys. Rev. B* **80**, 180414(R) (2009).
- [9] S. Pujari, K. Damle, and F. Alet, Néel-state to valence-bond-solid transition on the honeycomb lattice: evidence for deconfined criticality, *Phys. Rev. Lett.* **111**, 087203 (2013).
- [10] A. Nahum, P. Serna, J. T. Chalker, M. Ortuno and A. M. Somoza, Emergent SO(5) symmetry at the Néel to valence-bond-solid transition, *Phys. Rev. Lett.* **115**, 267203 (2015).
- [11] A. Nahum, J. T. Chalker, P. Serna, M. Ortuno and A. M. Somoza, Deconfined quantum criticality, scaling violations, and classical loop models, *Phys. Rev. X* **5**, 041048 (2015).
- [12] H. Shao, W. Guo, and A. W. Sandvik, Quantum criticality with two length scales, *Science* **352**, 6282 (2016).
- [13] H. Suwa, A. Sen, and A. W. Sandvik, Level spectroscopy in a two-dimensional quantum magnet: Linearly dispersing spinons at the deconfined quantum critical point, *Phys. Rev. B* **94**, 144416 (2016).
- [14] C. Wang, A. Nahum, M. A. Metlitski, C. Xu and T. Senthil, Deconfined quantum critical points: symmetries and dualities, *Phys. Rev. X* **7**, 031051 (2017).
- [15] Y. Q. Qin, Y. -Y. He, Y. -Z. You, Z. -Y. Lu, A. Sen, A. W. Sandvik, C. Xu, and Z. Y. Meng, Duality between the deconfined quantum-critical point and the bosonic topological transition, *Phys. Rev. X* **7**, 031052 (2017).
- [16] N. Ma, G.-Yu Sun, Y.-Z. You, C. Xu, A. Vishwanath, A. W. Sandvik, and Z. Y. Meng, Dynamical signature of fractionalization at a deconfined quantum critical point, *Phys. Rev. B* **98**, 174421 (2018).
- [17] G. Shreejith, S. Powell and A. Nahum, Emergent SO(5) symmetry at the columnar ordering transition in the classical cubic dimer model, *Phys. Rev. Lett.* **122**, 080601 (2019).
- [18] B. Zhao, P. Weinberg, and A. W. Sandvik, Symmetry-enhanced discontinuous phase transition in a two-dimensional quantum magnet, *Nature Physics* **15**, 678 (2019).
- [19] P. Serna and A. Nahum, Emergence and spontaneous breaking of approximate O(4) symmetry at a weakly first-order deconfined phase transition, *Phys. Rev. B* **99**, 195110 (2019).
- [20] J. Takahashi and A. W. Sandvik, Valence-bond solids, vestigial order, and emergent SO(5) symmetry in a two-dimensional quantum magnet, arXiv:2001.10045.
- [21] M. E. Fisher, in *Renormalization Group in Critical Phenomena and Quantum Field Theory*, J. Gunton and M. S. Green, Eds., (Temple University, 1975).
- [22] D. R. Nelson, Coexistence-curve singularities in isotropic ferromagnets, *Phys. Rev. B* **13**, 2222 (1976).
- [23] D. J. Amit and L. Peliti, On dangerously irrelevant operators, *Ann. Phys. (N.Y.)* **140**, 207 (1982).
- [24] F.-J. Jiang, M. Nyfeler, S. Chandrasekharan, and U.-J. Wiese, From an antiferromagnet to a valence bond solid: evidence for a first-order phase transition, *J. Stat. Mech.: Theory Exp.* **2008**, P02009 (2008).
- [25] S. Pujari, F. Alet, and K. Damle, Transitions to valence-bond solid order in a honeycomb lattice antiferromagnet, *Phys. Rev. B* **91**, 104411 (2015).
- [26] J. V. Jose, L. P. Kadanoff, S. Kirkpatrick, and D. R. Nelson, Renormalization, vortices, and symmetry-breaking perturbations in the two-dimensional planar model, *Phys. Rev. B* **16**, 1217 (1977).
- [27] A. V. Chubukov, S. Sachdev, and J. Ye, Theory of two-dimensional quantum Heisenberg antiferromagnets with a nearly critical ground state, *Phys. Rev. B* **49**, 11919 (1994).
- [28] S. Miyashita, Nature of the Ordered Phase and the Critical Properties of the Three Dimensional Six-State Clock Model, *J. Phys. Soc. Jpn.* **66**, 3411 (1997).
- [29] M. Oshikawa Ordered phase and scaling in Z_n models and the three-state antiferromagnetic Potts model in three dimensions, *Phys. Rev. B* **61**, 3430 (2000).
- [30] J. Hove and A. Sudbø, Criticality versus q in the (2+1)-dimensional Z_q clock model, *Phys. Rev. E* **68**, 046107 (2003).
- [31] J. Lou, A. W. Sandvik, and L. Balents, Emergence of U(1) Symmetry in the 3D XY Model with Z_q Anisotropy, *Phys. Rev. Lett.* **99** 207203 (2007).
- [32] T. Okubo, K. Oshikawa, H. Watanabe, and N. Kawashima, Scaling relation for dangerously irrelevant symmetry-breaking fields, *Phys. Rev. B* **91**, 174417 (2015).
- [33] M. Hasenbusch and E. Vicari, Anisotropic perturbations in three-dimensional O(N)-symmetric vector models, *Phys. Rev. B* **84**, 125136 (2011).
- [34] M. E. Zhitomirsky, P. C. W. Holdsworth, and R. Moessner, Nature of finite-temperature transition in anisotropic pyrochlore $\text{Er}_2\text{Ti}_2\text{O}_7$, *Phys. Rev. B* **89**, 140403(R) (2014).
- [35] F. Léonard, B. Delamotte, “Critical exponents can be different on the two sides of a transition: A generic mechanism”, *Phys. Rev. Lett.* **115**, 200601 (2015).
- [36] D. Banerjee, S. Chandrasekharan, and D. Orlando, Conformal Dimensions via Large Charge Expansion, *Phys. Rev. Lett.* **120**, 061603 (2018).
- [37] M. Hasenbusch, Monte Carlo study of an improved clock model in three dimensions *Phys. Rev. B* **100**, 224517 (2019).
- [38] H. Shao, W. Guo, A. W. Sandvik, Monte Carlo renormalization flows in the space of relevant and irrelevant operators: Application to three-dimensional clock models, *Phys. Rev. Lett.* **124** 080602 (2020).
- [39] J. Cardy, *Scaling and Renormalization in Statistical Physics*, Cambridge University Press (Cambridge, 1996).
- [40] S. R. Shenoy and B. Chattopadhyay, Anisotropic three-dimensional XY model and vortex-loop scaling, *Phys. Rev. B* **51**, 9129 (1995).
- [41] T. Senthil, L. Balents, S. Sachdev, A. Vishwanath, and M. P. A. Fisher, Quantum criticality beyond the Landau-Ginzburg-Wilson paradigm, *Phys. Rev. B* **70**, 144407 (2004).

- [42] It may appear puzzling why essentially correct results for the exponents ν_q were obtained in Ref. [31] even though the assumption made for the overall L dependence was incorrect for the regime of L and t used for data collapse as a function of $tL^{1/\nu}$. The reason may be that the exponent $\sigma\beta/\nu \approx 0.5$ is not very large, and the data collapse was observed where ϕ_q already approaches its maximal value $\phi_q = 1$. In this regime, a different scaling form applies [32, 38] (as also discussed in the present paper), where the values of ϕ_q should not be rescaled at all, i.e., $L^\sigma \phi_q$ with $\sigma = 0$ should be used. Since the value $\sigma = 0.52$ actually used in Ref. [31] is not very large, the scaling collapse still worked the best when ν_q was close to its correct value. Thus, the reasonable results obtained were in part due to fortuitous circumstances, which may not have applied to Ref. [34], where the same assumptions were made.
- [43] D. Banerjee, S. Chandrasekharan, and D. Orlando, Conformal dimensions via large charge expansion, *Phys. Rev. Lett.* **120**, 061603 (2018).
- [44] M. Campostrini, M. Hasenbusch, A. Pelissetto, P. Rossi, and E. Vicari, Critical behavior of the three-dimensional XY universality class, *Phys. Rev. B* **63**, 214503 (2001).
- [45] K. Binder, Finite size scaling analysis of Ising model block distribution functions, *Z. Phys. B* **43**, 119 (1981).
- [46] J. M. Luck, Corrections to finite-size-scaling laws and convergence of transfer-matrix methods, *Phys. Rev. B* **31**, 3069 (1985).
- [47] J. E. Cohen, S. Friedland, T. Kato, and F. P. Kelly, Eigenvalue inequalities for products of matrix exponentials, *Linear Algebra Appl.* **45**, 55 (1982).
- [48] F. Taherkhani, H. Akbarzadeh, H. Abroshan, S. Ranjbar, A. Fortunelli, and G. Parsafar, Study of two dimensional anisotropic Ising models via a renormalization group approach, *Physica A* **392**, 5604 (2013).
- [49] N. K. Kultunov and Y. E. Lozovik, The vortex-loop phase transition in the anisotropic 3D XY model: The role of screening and the polymer physics approach, *Physica Scripta*, **56**, 129 (1997).
- [50] A. K. Nguyen and A. Sudbø, Phase coherence and the boson analogy of vortex liquids, *Phys. Rev. B* **58**, 2802 (1998).
- [51] S.-Z. Lin, X. Wang, Y. Kamiya, G.-W. Chern, F. Fan, D. Fan, B. Casas, Y. Liu, V. Kiryukhin, W. H. Zurek, C. D. Batista and S.-W. Cheong, Topological defects as relics of emergent continuous symmetry and Higgs condensation of disorder in ferroelectrics, *Nature Physics* **10**, 970977 (2014).
- [52] F. Xue, N. Wang, X. Wang, Y. Ji, S.-W. Cheong, and L.-Q. Chen, Topological dynamics of vortex-line networks in hexagonal manganites, *Phys. Rev. B* **97**, 020101(R) (2018).
- [53] A. W. Sandvik, Stochastic series expansion method for quantum Ising models with arbitrary interactions, *Phys. Rev. E* **68**, 056701 (2003).
- [54] T. Surungan, S. Masuda, Y. Komura, Y. Okabe, Berezinskii-Kosterlitz-Thouless transition on regular and Villain types of q-state clock models, *J. Phys. A: Math. Theor.* **52**, 275002 (2019).
- [55] T. Senthil and S. N. Majumdar, Critical properties of random quantum potts and clock models, *Phys. Rev. Lett.* **76**, 3001 (1996).
- [56] E. Carlon, P. Lajkó, and F. Iglói, Disorder induced cross-over effects at quantum critical points, *Phys. Rev. Lett.* **87**, 277201 (2001).
- [57] F. Hrahsheh and T. Vojta, Disordered bosons in one dimension: From weak-to strong-randomness criticality, *Phys. Rev. Lett.* **109**, 265303 (2012).